Original Article

Novel albendazole-glucan particles for enhancing intestinal absorption and improving hepatic targeting

Yan Liu[1#], Haishan Yang[1#^], Jihai Zhu[2], Zufan Yang[1], Lingli Zhao[3], Xiang Zhang[3], Haixia Zhang[4]

[1]Basic Medical Research Center, School of Medicine, Qinghai University, Xining, China; [2]Cardiothoracic Surgery Department, Affiliated Hospital of Qinghai University, Xining, China; [3]Laboratory Department, Affiliated Hospital of Qinghai University, Xining, China; [4]Digestive Department, Affiliated Hospital of Qinghai University, Xining, China

Contributions: (I) Conception and design: None; (II) Administrative support: None; (III) Provision of study materials or patients: None; (IV) Collection and assembly of data: X Zhang; (V) Data analysis and interpretation: H Yang; (VI) Manuscript writing: All authors; (VII) Final approval of manuscript: All authors.

[#]These authors contributed equally to this work.

Correspondence to: Yan Liu. Basic Medical Research Center, School of Medicine, Qinghai University, 251 Ningda Road, Xining, China. Email: liuyan20190307@163.com.

Background: Glucan particles (GPs) are derived from the *Saccharomyces cerevisiae* cell wall. The hollow particles composed of β-1,3-D-glucan have been extensively studied in terms of immune regulation and macrophage-targeted drug delivery. Albendazole (ABZ) is a benzimidazole drug with good anti-parasitic activity and is the drug recommended by the World Health Organization for the first-line treatment of hydatid disease.

Methods: A dynamic light scatterometer, scanning electron microscope, and transmission electron microscope were used to characterize the ABZ-GPs. High-performance liquid chromatography (HPLC), laser scanning confocal microscope (LSCM) and an *in vivo* small animal imaging system were used to evaluate theability of ABZ-GPs to be recognized by macrophages, whether ABZ-GPs are more readily absorbed and eliminated in the blood than the original ABZ drug in rats, and the ability of ABZ-GPs to target the mouse liver.

Results: The ABZ-GPs were successfully constructed to achieve fluorescence, magnetic resonance imagining, and laser confocal microscopy imaging. The glucan shell effectively protects ABZ from enzymatic degradation and from being pumped out in the gastrointestinal tract. The analysis of ABZ and its major metabolite albendazole sulfoxide in the rat plasma and mouse liver showed that compared to the ABZ suspension group, the degradation of ABZ-GPSs in the blood was low, and the targeting of ABZ-GPSs in the liver was significantly enhanced.

Conclusions: In the oral treatment of hepatic hydatid disease, GPs can be used as carriers to achieve the targeted transport of ABZ, which in turn can be used for the targeted therapy of liver echinococcosis. Thus, ABZ-GPs may be a promising form of targeted therapy.

Keywords: Glucan nanoparticle; albendazole; pharmacokinetics; liver targeting; hydatid disease

Submitted Sep 20, 2022. Accepted for publication Nov 29, 2022.

doi: 10.21037/atm-22-5299

View this article at: https://dx.doi.org/10.21037/atm-22-5299

^ ORCID: 0000-0002-7882-5315.

© Annals of Translational Medicine. All rights reserved.

Introduction

Hydatid disease, which is a serious zoonotic parasitic disease caused by hydatid tapeworm parasitism in humans and certain animals (1), has become a global public health and economic issue. It can be divided into cystic echinococcosis and alveolar echinococcosis (AE), which are caused by the eggs of *Echinococcus granulosus* and *Echinococcus multilocularis*, respectively (2). *Echinococcus multilocularis* is caused by the infection of multilocular cysts and readily adheres to the surrounding tissue. The site of the lesion is unstable, and the cysts easily spread, forming AE. Thus, the treatment of AE, which is also called "parasitic cancer," is difficult and is related to strong pathogenicity, disability, and high mortality (3). If it is not treated in time, the 10-year mortality rate is as high as 94% (4). Thus, the treatment of echinococcosis has become an important issue related to national health, and a social challenge that must be addressed urgently.

Currently, surgery is the first choice for curing echinococcosis; however, the parasite spreads easily during the operation and thus echinococcosis frequently recurs. In addition, echinococcosis has no significant clinical symptoms in the early stage, and the diagnosis lacks specificity, making it difficult to diagnose and treat. Patients that progress to the middle and late stages of the disease are often ineligible for the surgical intervention. Thus, drug chemotherapy has received increasing attention (5). At present, anti-hydatid drugs mainly include anti-parasitic drugs, anti-cancer proliferation drugs, and herbal medicine. Among them, albendazole (ABZ) is the most commonly used drug for treatment due to its good intestinal absorption and low price. However, studies have shown that ABZ is poorly absorbed in the gastrointestinal tract (GIT) via oral administration due to its low solubility and systematic distribution in the body. Thus, new ABZ preparations, such as emulsions, liposomes, freeze-dried powders, chitosans, nanoparticles, and salts (6-9) have been used to improve anti-parasitic efficacy and bioavailability. However, most of these forms of ABZ have not been used clinically.

Research has shown that ABZ emulsions are better suited for use in clinical settings than ABZ tablets (10); however, certain limitations persist, including poor stability, low solubility, off-target effects, and adverse reactions. Thus, biosafe and targeted drug delivery systems need to be developed that are capable of preventing the drug from being degraded, while also limiting non-specific absorption during the *in vivo* delivery of drugs. The development of biosafe and targeted drug delivery systems has become a trend in drug therapy delivery systems. The targeted delivery of drugs to hydatid lesions can improve therapeutic efficacy and reduce the side effects of the drugs.

Glucan particles (GPs) are derived from *Saccharomyces cerevisiae*. The β-1,3-D-glucan primarily forms spherical hollow particles 2–5 μm in diameter (11,12). In addition to being used as drug carriers, these particles can also regulate auto-immune activity, thereby affecting immune cells and exerting a certain synergistic effect with general anti-inflammatory, antioxidant, and anti-tumor responses (13). As carriers, their unique structure, including their large hollow space, can be loaded with various particles, including peptides and proteins. Although the cell wall-derived β-1,3-D glucan has some shortcomings, such as low content (1–7%), high viscosity and complex production process (14). But the more importantly, β-1,3-D-glucan retains the ability to be recognized and phagocytosed, even after drug encapsulation (15). The β-1,3-D-glucan is the main pathogen-associated molecular pattern of fungi, and it can be recognized by the dectin-1 (16), complement receptor 3 (CR3) (17), and scavenger receptor (18), which makes it a targeting vector for macrophages. Additionally, the human GIT lacks β-amylase (19) prevents the drugs loaded in the

Highlight box

Key findings

- Novel albendazole-glucan particles can be used for the targeted treatment of patients with hepatic echinococcosis.

What is known and what is new?

- Albendazole is recommended by WHO as the first choice chemotherapy drug for the treatment of Echinococcus echinococcus disease, but its low solubility and wide distribution *in vivo* greatly affect its absorption and bioavailability, which is one of the reasons why ABZ has poor efficacy in treating parenteral parasitic diseases such as liver hydatids.
- In this study, we used β-1,3-D-glucan, which has good biocompatibility and can be used as a macrophage targeting vector, as the carrier of albendazole. Novel albendazole glucan nanoparticles were prepared to improve the liver targeting and bioavailability of albendazole.

What is the implication, and what should change now?

- The Novel albendazole-glucan particles has good liver targeting and is a promising targeted therapy for hepatic echinococcosis. Therefore, it is necessary to do further research on the efficacy and extend it to the clinic.

© Annals of Translational Medicine. All rights reserved.

GPs from being digested and pumped out when passing through the GIT. β-glucans have been extensively studied in terms of their immunomodulation and anti-inflammatory effects (20), and as drug carriers. Notably, β-glucans specifically identifies macrophages and has been used to transfer payload macromolecules; that is, protein (21,22), deoxyribonucleic acid (DNA) (23,24), small-interfering ribonucleic acid (25), and small drug molecules (e.g., rifampicin, methotrexate, and curcumin] (26-28). They have also been studied in the context of hepatitis B therapy (29), Francisella vaccines (30), and as a new tool in vaccine development (31,32).

We previously reported changes in the basic morphological structure of the tissue surrounding the liver lesions of secondary hydatid mice, and found that the basic morphological structure of the tissues surrounding the hepatic alveolar hydatid lesions changed, and a large number of inflammatory cells were infiltrated around the central veins and portal areas. Additionally, a large number of large macrophages were found in the splenic bodies and lymphatic sheath around the splenic arteries. Wang (33) reported significant inflammatory cell infiltration in the marginal zone of the liver tissue in patients with hepatic AE, in whom the number of macrophages increased significantly and the proportion of M2 macrophages also increased.

Compared with anti-hydatid drugs in previous studies, in this study, GPs with good biocompatibility, unique hollow structure and easy absorption and degradation were used as drug carrier. GPs can be specifically recognized and captured by glucan receptors (such as Dectin-1 or CR3) on the surface of macrophages, to make drugs have certain characteristics of targeting, we investigated whether GPs could be used as a carrier for ABZ, targeting ABZ to hydatid disease-prone sites to achieve a targeted treatment of echinococcosis. We present the following article in accordance with the ARRIVE reporting checklist (available at https://atm.amegroups.com/article/view/10.21037/atm-22-5299/rc).

Methods

Reagents, drugs, and animals

ABZ (lot no. MKCB9477) was obtained from Sigma-Aldrich (New Jersey, United States). The GPs were purified in our laboratory. The dialkylcarbocyanines (DiRs) were provided by Maokangbio (Shanghai, People's Republic of China). All the other chemicals were of analytical grade and were obtained from Oubokai (Tianjin, People's Republic of China).

We used a Thermo Q Exactive Fourier Transform Ultra-High Resolution LC/MS to record chromatograms, which was set at 296 nm. The reversed-phase column was AccuCORE aQ (2.1 mm × 150 mm, 5 μm), which was thermostatic at 35 ℃. The mobile phase was a mixture of acetonitrile and 1% formic acid water, and the flow rate was 0.3 mL/min. The ultrastructure observation of ABZ-GPs was performed using Hitachi S-4800 field emission scanning electron microscopy and a FEI Tecnai G220 S-TWIN. A Zeiss LSM780 laser confocal microscope was used to observe the ABZ-GPs engulfed by the macrophages. A platinum Elmer IVIS Spectrum CT small animal *in vivo* 3-dimensional (3D) multi-modal imaging system was used to observe the tissue and organ distribution of the ABZ-GPs in the mice.

Kunming rats (male, weighing 200±5 g) and Kunming mice (male, weighing 20–25 g) were provided by the Experimental Animal Management Center, School of Medicine, Xi'an Jiaotong University. All the animals were housed in a temperature controlled (25±2 ℃) and 12-h light/dark-cycled room with *ad-libitum* access to food and water. Animal experiments were approved by the Research Ethics Committee of the Affiliated Hospital of Qinghai University (approval No. AF-RHEC-0062-01) and in compliance with institutional guidelines for the care and use of animals. All animals were euthanized at the end of the experiment. A protocol was prepared before the study without registration.

Preparation of GPs

GPs are a Food and Drug Administration (FDA)-approved food additive. Commercialized products are currently available on the market, such as the nutritional supplement Welmune produced by Biothera. Commercially used GPs for research are also available, such as the WGP dispersible (InvivoGen, San Diego, CA, USA). In this study, we used our own purified product. After purchasing live yeast (*Saccharomyces cerevisiae*, Baker's Yeast), we cultivated it to the logarithmic growth phase before extraction. From our experience, the uniformity and original biological activity of the GPs obtained in this way can be better maintained.

An acid-base treatment was adopted for the extraction (34). First, the live yeast in the logarithmic growth phase was separated from the medium by centrifugation at 8000 ×g for 20 min, and the supernatant was discarded; a 1-M Sodium Hydroxide (NaOH) aqueous

© Annals of Translational Medicine. All rights reserved.

solution was prepared fresh and heated to 80 ℃. Next, the live yeast obtained by centrifugation was dispersed in 100 mL of hot NaOH solution and stirred at 80 ℃ for 1 h. After the treatment, the solution was centrifuged at 7550 ×g for 5 min to collect the insoluble components and washed 3 times in 100 mL of Milli-Q water to remove the NaOH and substances decomposed by the hot lye. The pH value of 100 mL of the solution was then adjusted to 5.0 with hydrochloric acid (HCl), and stirred continuously for 1 h at 55 ℃. The insoluble matter was collected by centrifugation at 7550 ×g, washed 2 times with Milli-Q water, 4 times with 50 ml of isopropanol, and 2 times with acetone, and all the solvents were vacuum dried to obtain the GPs, which were stored at –20 ℃.

Preparation of ABZ-GPs

Equimolar amounts of diethylenetriaminepentaacetic acid (DTPA) and gadolinium nitrate ($Gd(NO_3)_3 \cdot 6H_2O$) were dissolved in 20 ml of ultrapure water and ultrasonicated for 2 h at 25±1 ℃ to form a stable Gd^{3+}-DTPA complex. The carboxyl group of DTPA was first activated by an equimolar amount of 1-ethyl-3-(3-dimethylamino-propyl) carbodiimide/N-hydroxysuccinimide for 2 h. The pH was then adjusted to 8.0 before bovine serum albumin (BSA) was added; the solution was stirred overnight in the dark. For each 0.1 mmol of the Gd^{3+}-DTPA complex, 20 mg of BSA was added. An activated dialysis bag (with a molecular weight cut-off of 25 kD) was then used to perform the dialysis in pure water for 48 h. The water was changed every 2 h for the first 12 h, and then every 6 h to remove the unreacted molecules. The dialysis product was lyophilized to obtain the Gd^{3+}-DTPA-modified BSA.

After 50 mg of ABZ had been fully dissolved in glacial acetic acid, it was lyophilized to form a dry powder. Next, 25 micrograms of DiR and 20 mg Gd^{3+}-DTPA-modified BSA were dissolved in 100 µl of pure water, mixed at room temperature (25±1 ℃), and protected from light for 1 h, transferred to a tube of 50 mg of ABZ lyophilized powder, supplemented with 100 µL of 2-Morpholinoethanesulfonic acid buffer (pH=3.8), and the solution was mixed at 600 rpm at room temperature for 4 h in the dark. Subsequently, the liquid was transferred to 50 mg of a freeze-dried dextran particle powder, mixed at 600 rpm at room temperature, and protected from light for 6 h, washed with Tris-HCI (pH =7.5) twice, then washed with ultrapure water thrice, and subsequently lyophilized overnight. Once the lyophilized powder had been infiltrated with 50 µL of pure water for 30 min, 50 µL of tetrahydrofuran was added, after which the solution was vortexed and then left to stand at room temperature for 30 min, and then lyophilized again for 48 h to completely remove water and tetrahydrofuran.

Surface potential and particle size of Gd3+-DTPA@BSA

Deionized water was used to prepare a NaCl solution with a concentration of 0.01 mol/L, which was filtered through a 0.22 µm sterile filter membrane. A certain amount of lyophilized Gd^{3+}-DTPA@BSA was drawn off and dissolved in the prepared NaCl solution, and ultrasonic waves were used for intermittent treatment to fully mix the Gd^{3+}-DTPA@BSA. A small amount of Gd^{3+}-DTPA@BSA was spotted on silicon wafers, then sputtered for 10 s with gold, and a scanning Hitachi S-4800 field emission scanning electron microscopy was used for the observations at 10 kV. A Malvern Zetasizer ZS90 Dynamic light scattering instrument was used for the detection.

SEM imaging of empty GPs and ABZ-GPs

Following the swelling of 1 mg of GPs or ABZ-GPs with pure water, 1 µL was aliquoted, and diluted 100–100,000 times. Next, 10 µL of each solution was dropped onto high-purity silicon wafers and dried. The samples were then placed in a vacuum plasma generator and sprayed with gold for 1 min, fixed on the sample stage of the scanning electron microscope (SEM) with conductive tape, and photographed with a Hitachi S-4800 field emission SEM.

TEM imaging of empty GPs and ABZ-GPs

After the loaded 2 mg of ABZ-GPs were fully swelled with 20 µL of pure water, an appropriate amount of electron microscope grade glutaraldehyde reagent was added to the final concentration of the solution 2.5% (w/v) and allowed to crosslink at room temperature for 1 h. After washing with ultrapure water thrice, the samples underwent critical point carbon dioxide (CO_2) dehydration. Next, electron microscope epoxy resin was embedded for 30 min before the samples were oven-cured at 60 ℃ for 24 h. After the solidified sample block had been trimmed, it was cut with an ultra-thin microtome into 70 nm-thick slices. The slices were then stained with 5 µL of saturated uranyl acetate for 30 s, washed twice with pure water, and fully dried before being photographed with a FEI Tecnai G220 S-TWIN transmission electron microscope (TEM).

© Annals of Translational Medicine. All rights reserved.

ABZ-GP centrifuge tube fluorescence imaging

To assess whether ABZ binds to the fluorescent dye DiR, which excites at 750 nm and emits at 780 nm, 1 mg of the loaded ABZ-GPs was swelled with pure water and added to 1 ml of water to form tube No. 3. The ABZ-GPs were also diluted 10× to form tube No. 2. The empty GPs and BSA that had been swollen with pure water were used as control tube (No. 1). The 3 tubes were placed on a small animal imaging system to capture photographs and observe fluorescence.

ABZ-GP laser confocal microscope imaging

To observe the condition of the ABZ carried by the GPs, tube No. 3 was centrifuged at 7,550 ×g for 5 min. The supernatant was then discarded, and 1 mL of dichlorotriazinyl amino fluorescein (DTAF) staining solution (0.25 mg/mL of sodium carbonate buffer or phosphate buffer, pH=8) was added. Next, the product was stained at room temperature for 6 h and washed with ultrapure water thrice. Next, 1 mL of pure water was added to fully suspend the product before 20 μL was aliquoted onto a glass slide, which was then mounted with a cover glass to be viewed under a Zeiss LSM780 confocal laser microscope.

Release of ABZ by ABZ-GPs in vitro

The ABZ-GPs (10 mgs) and phosphate buffer (10 mL, pH=2.0 and 8.0) were shaken well at 60 rpm at room temperature. At the designated time points (0.25, 0.5, 1, 2, 6, 12, 24, 36, 48, 72, and 96 h) 1 mL of supernatant was aliquoted, 1 mL of fresh buffer was added, and the solution was shaken well. The supernatant was collected to measure the ultraviolet absorption (296 nm) of ABZ, and the amount of ABZ released was calculated using a pre-measured ABZ ultraviolet absorption-concentration standard curve.

Phagocytosis of ABZ-GPs by macrophages in vitro

RAW264.7 mouse macrophages (1×10^4 cells) were inoculated into Dulbecco's modified Eagle medium glass-bottom small dishes containing 10% fetal bovine serum and glucose, which were then placed into a humidified incubator for overnight culture at 37 ℃ with 5% CO_2. The following day, the ABZ-GPs were dispersed, and 0.1 mg was aliquoted and diluted into the culture medium. The macrophages were then added to a small dish and incubated at 37 ℃. The ABZ-GPs were removed after 1, 2, and 4 h, washed thrice with phosphate buffered saline (PBS) to remove GPs that had not phagocytosed, fixed with 4% paraformaldehyde at room temperature for 10 min, washed thrice with PBS to remove excess paraformaldehyde, and imaged using a ZEISS LSM780 laser confocal microscope to observe phagocytosis.

ABZ-GPs were phagocytosed by macrophages in the small intestine and liver tissues

Before euthanasia by cervical dislocation, 50 mg/kg of the ABZ-GPs was administered to the healthy Kunming mice by oral gavage for 2 h. The fluorescently stained mouse liver and small intestine sections (approximately 0.2–0.5 cm^3) were then collected, rinsed with PBS, and fixed with 10% formalin for 1 h. Next, the excess formalin fixative was washed off with PBS, and the tissues were embedded with optimal cutting temperature (OCT) compound, fixed with liquid nitrogen, transferred to a cryostat, and cut into 6-μm thick sections. The sections were then transferred to an anti-detachment glass slide for adhesion. The adhered sections were permeabilized and blocked with PBS containing 0.3% Triton X-100 and 3% BSA, at room temperature for 1 h. The membrane solution was discarded, 3% BSA in PBS with 0.05% Tween 20 (PBST) containing anti-F4/80 primary antibody (ab6640, diluted 500 times) was added, and the mixture was protected from light overnight at 4 ℃. The next day, the primary antibodies were discarded while the remainder was washed with PBST 5 times and blocked with 3% BSA in PBST for 20 min. Next, the Alexa Fluor 488-labelled goat anti-rabbit secondary antibody (ab150165, diluted 1:1,000) was added. The mixture was incubated at room temperature for 1 h in the dark and washed 5 times with PBST, after which 2 μg/mL of 4',6-diamidino-2-phenylindole (DAPI) PBS solution was added for staining for 10 min at room temperature. Finally, the slide was washed twice with PBS and mounted with a cover glass (Gold Antifade mount), and the images were then captured with a Zeiss LSM780 microscope.

Pharmacokinetic behaviors and liver targeting of the formulations

As the preferred anti-hydatid drug, ABZ has a very fast metabolic rate in plasma (35). After oral administration,

© Annals of Translational Medicine. All rights reserved.

ABZ is rapidly transformed into ABZ sulphoxide (ABZSO) and $ABZSO_2$ (of which ABZSO is the main active substance) and finally into albendazole-2-aminosulfone ($ABZSO_2$-NH_2) under the action of various enzyme systems in the liver (36). Thus, ABZ and ABZSO were selected for the study of the pharmacokinetic index in our research.

The 20 rats (male, 7 weeks old, 200±20 g) were randomly divided into 2 groups. The rats were fasted with access to water for 12 h before the oral gavage and were given a single dose of 50.0 mg/kg of ABZ suspension or ABZ-GPs before the oral administration, respectively. Before administration (0 h) and after administration (0.5, 1, 2, 4, 6, 8, 12, and 24 h) approximately 0.5 mL of blood was collected from the fundus venous plexus, placed in a heparinized centrifuge tube, and centrifuged at 11,544 ×g for 5 min to separate the plasma. Next, 100 microliters of the plasma supernatant was aspirated into a centrifuge tube, an equal volume of methanol was added, and the mixture was vortexed for 1 min, and centrifugated at 11,544 ×g for 5 min. Subsequently, 100 µL of the supernatant was aspirated into a centrifuge tube. An equal amount of the internal standard solution was added, and the mixture was vortexed for 1 min and centrifuged at 11,544 ×g. Next, the supernatant was collected and filtered through a microporous membrane (0.22 µm).

The 100 Kunming mice (male, 6 weeks old, 30±3 g) were randomly divided into 2 groups. The mice were fasted with access to water for 12 h before the administration of a single dose of 15.0 mg/kg of ABZ suspension or ABZ-GPs, respectively. Before intragastric administration (0 h) and after administration (0.5, 1, 2, 4, 6, 8, 12, and 24 h), 5 mice were euthanized, and their livers were excised and placed in a petri dish. Each liver surface was rinsed with sterile normal saline. Next, 5 g of the liver tissue was weighed, cut into pieces with scissors, placed in a homogenizer, and 1.0 mL of saline was added. The mixture was homogenized at 500 rpm for 5 min, centrifuged at 11,544 ×g for 5 min, and 0.5 mL of the supernatant was aspirated and centrifuged. Next, 1 milliliter of PBS was added to the tube, which was vortexed for 1 min. After centrifugation, 0.5 mL of the supernatant was pipetted into a centrifuge tube, and the same amount of methanol was added for extraction. The same amount of internal standard was then added, after which the mixture was vortexed for 1 min, homogenized, and centrifuged at 11,544 ×g. The supernatant was adsorbed and filtered through a microporous membrane (0.22 µm).

The ABZ and ABZSO in the rat plasma and mouse liver tissue homogenate were determined by liquid chromatography-high-resolution mass spectrometry (LC-MS/MS). The chromatographic conditions were as follows: an AccuCORE aQ column was used (150 mm × 2.1 mm, 5 µm); the column temperature was 35 ℃, injection volume 0.2 µL, flow rate 0.3 mL/min, detection time 10 min, and the mobile phase was a methanol: formic acid water solution (0.1%). The mobile phase was subjected to gradient elution according to the following protocol: 0.0–5.0 min: 45% methanol, 55% formic acid water; 5.0–6.0 min: 45–90% methanol, 45–10% formic acid water; 6.0–7.0 min: 90%methanol, 10% formic acid water; 7.0–8.0 min: 90–45% methanol, 10–45% formic acid water; 8.0–10.0 min: 45% methanol, 45% formic acid water. The mass spectrometry conditions were as follows: full MS scan mode, electrospray ion source (ESI); carrier gas: high-purity nitrogen (purity >99.9 %), sheath gas flow rate 35 units, auxiliary gas flow rate 15 units, purge gas flow rate 0 units; spray voltage 3.0 kV; capillary temperature 320 ℃, ion lens voltage frequency (S-lens RF level) 50; auxiliary gas heat source temperature 350 ℃; positive ion scan mode. The pharmacokinetic parameters were then computed using the WinNonLin software (version 8.2).

In vivo near-infrared fluorescence real-time imaging

DiR is a long-chain lipophilic DiR and environmentally sensitive fluorescent dye. When it is combined with membranes or with lipophilic molecules (such as proteins), the fluorescence intensity is significantly enhanced (although the fluorescence intensity of proteins is weak in water). Once in the cell, DiR gradually diffuses in the endoplasmic reticulum of the cell, and the entire cell can be evenly stained under the optimal concentration conditions (37).

The DiR-labelled ABZ-GPs were administered to the 3-week-old mice by gavage for 5consecutive days. The mice were anaesthetized with isoflurane 2 h after oral gavage on the 5th day. An IVIS Spectrum computed tomography near-infrared fluorescence imaging system was used to capture the 2D and 3D images to determine the targeting ability of the ABZ-GPs.

Statistical analysis

Using SPSS (version 20.0; IBM, Armonk, NY, USA), the pharmacokinetic parameters of the ABZ and ABZ-GP groups were compared by a 1-way analysis of variance. P values <0.05 were considered statistically significant.

© Annals of Translational Medicine. All rights reserved.

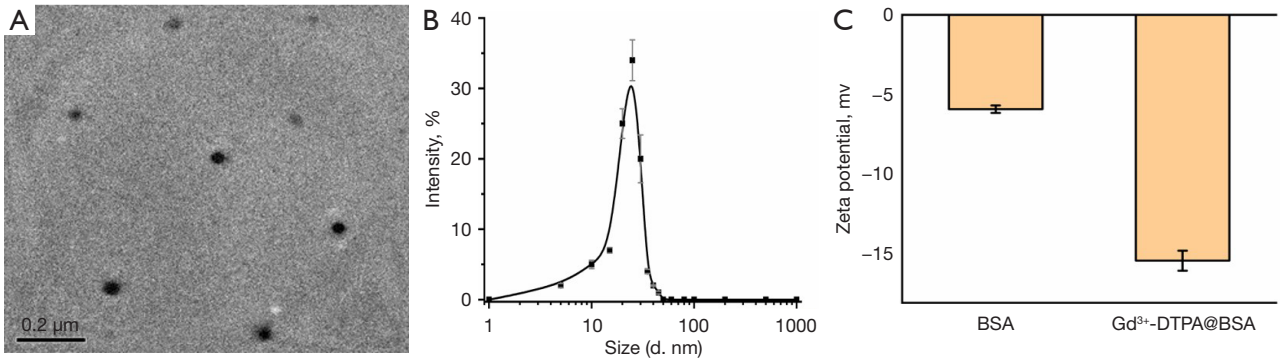

Figure 1 BSA and Gd^{3+}-DTPA@BSA. (A) SEM image of Gd^{3+}-DTPA@BSA, scale bar =0.2 μm. (B) Gd^{3+}-DTPA@BSA particle size distribution diagram. (C) Zeta potential of BSA and Gd^{3+}-DTPA@BSA. BSA, bovine serum albumin; DTPA, diethylenetriaminepentaacetic acid; SEM, scanning electron microscope.

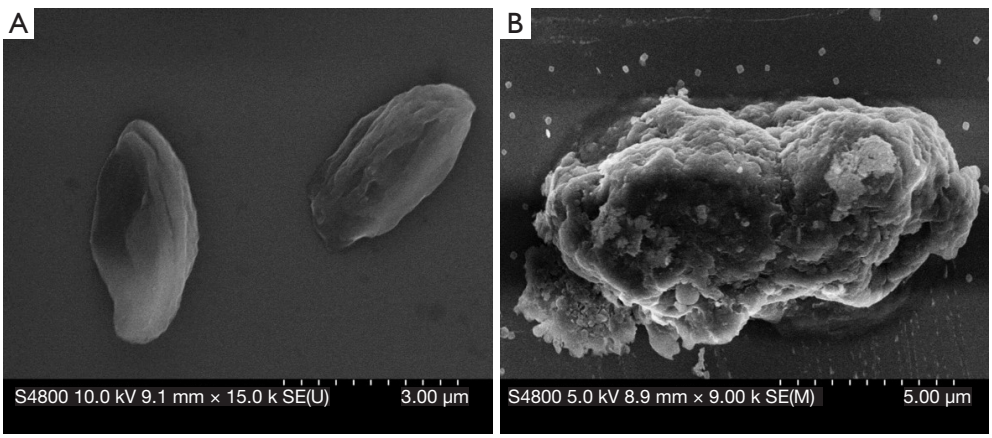

Figure 2 The ultrastructure of GPs and GP loaded with ABZ were detected by a scanning electron microscope. (A) SEM image of an empty GP; scale bar =3.0 μm; (B) GPs loaded with ABZ; scale bar =5.0 μm. SEM, scanning electron microscope; GPs, glucan nanoparticles; ABZ, albendazole.

Results

Physicochemical characteristics of Gd3+-DTPA@BSA

We detected the particle size and surface potential of Gd^{3+}-DTPA@BSA with a Malvern Zetasizer ZS90 and Hitachi S-4800 field emission scanning electron microscopy. As *Figure 1A* shows, the microscopic image of the Gd^{3+}-DTPA@BSA (0.2 um) shows a uniform distribution. As *Figure 1B* shows, the Gd^{3+}-DTPA@BSA had a mean particle size of 23.8±2.27 nm and a narrow size distribution. The $Gd3^{+}$-DTPA@BSA had a mean zeta potential of –15.37±0.62 mv, while that of BSA was –5.90±0.23 mv (see *Figure 1C*).

Imaging of GPs and ABZ-GPs by SEM and TEM

We used a Hitachi S-4800 field emission SEM (*Figure 2*) and FEI Tecnai G220 S-TWIN TEM (*Figure 3*) to observe the ultramicroscopic morphology of the constructed ABZ-GPs. In the SEM image, compared to the empty GPs, a large amount of ABZ adhered to the surface of the GPs, which increased the volume of the ABZ-GPs. In the TEM image, the hollow structure of the GPs was filled with white epoxy resin, while the hollow structure of the ABZ-GPs was filled with black drugs, which were fully loaded and evenly distributed. Thus, we confirmed that GPs can carry ABZ.

© Annals of Translational Medicine. All rights reserved.

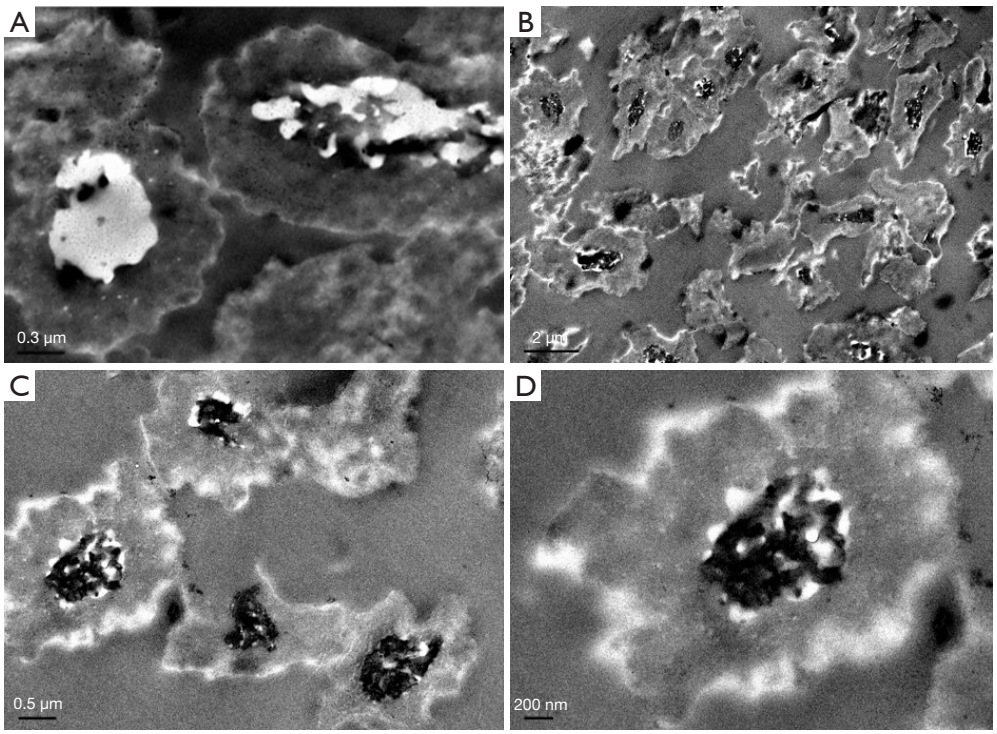

Figure 3 The ultrastructure of GPs and GPs loaded with ABZ were detected by a transmission electron microscope. (A) TEM image of an empty GP; scale bar =0.3 μm; (B) GPs loaded with ABZ; scale bar =2.0 μm; (C) GPs loaded with ABZ; scale bar =0.5 μm; (D) GPs loaded with ABZ; scale bar =200.0 nm. TEM, transmission electron microscope; GPs, glucan nanoparticles; ABZ, albendazole.

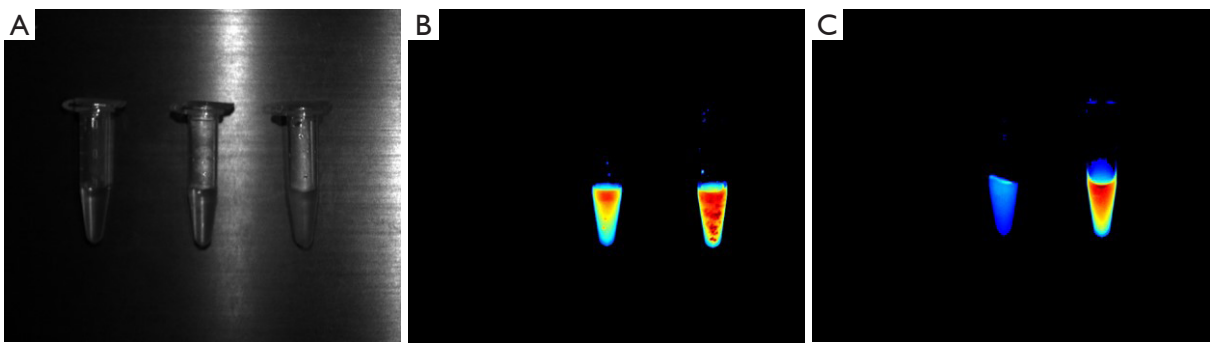

Figure 4 Fluorescence imaging of empty GPs and GPs loaded with ABZ in centrifuge tubes swollen in pure water; 1: empty GPs, 2: 0.1 mg/mL of GPs loaded with ABZ, 3: 1 mg/mL of GPs loaded with ABZ. (A) Before imaging, (B) imaging after 1 h, (C) imaging after 12 h. GPs, glucan nanoparticles; ABZ, albendazole.

ABZ-GP centrifuge tube fluorescence imaging

We filled the empty GPs (A, 1), and diluted the GPs loaded with ABZ 10× (A, 2) and the GPs loaded with ABZ (A, 3) with 0.5 ml of pure water (*Figure 4*). After placing them in the small animal imaging system, no fluorescence was observed in tube1 (blank), but fluorescence was observed in tubes 2 and 3 (the ABZ-GPs). Moreover, an increase in the concentration, led to an increase in the fluorescence intensity (B). After tubes 2 and 3 were kept at room temperature for 6 h, the fluorescence of tube 2 was substantially weakened and only the blue fluorescence remaining. The fluorescence intensity of tube 3 was also

© Annals of Translational Medicine. All rights reserved.

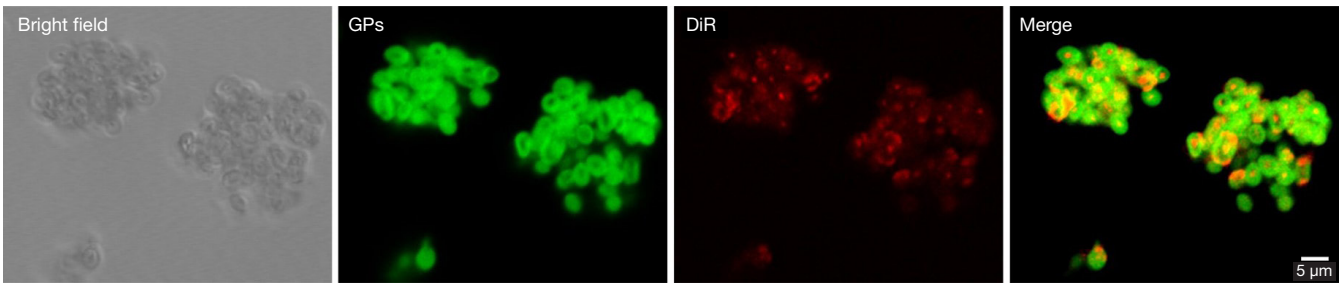

Figure 5 Confocal images of DTAF-labelled GPs loaded with fluorescent DiR-labelled ABZ-Gd^{3+}-DTPA@BSA; scale bar =5 μm. GPs, glucan nanoparticles; DTAF, dichlorotriazinyl amino fluorescein; ABZ, albendazole; DTPA, diethylenetriaminepentaacetic acid; BSA, bovine serum albumin.

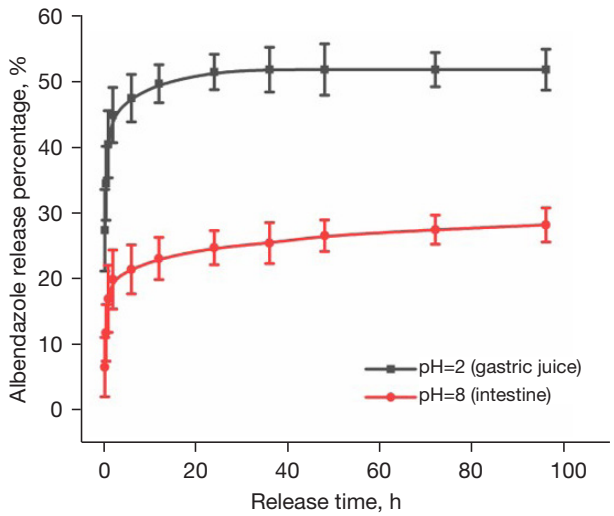

Figure 6 Drug release curve of ABZ-GPs at gastric and intestine pH values. ABZ-GPs, albendazole-glucan nanoparticles.

remarkably weakened (C).

ABZ-GP laser confocal microscope imaging

We analyzed the dual-colour fluorescent ABZ-GPs with a Zeiss LSM780 confocal microscope (*Figure 5*). For the imaged GPs, each pixel of red fluorescence was enclosed within a region of green fluorescence, which confirmed that ABZ had been successfully loaded into the GPs. However, before the ABZ-GPs could be used for further experiments, we needed to determine whether the GPs could carry ABZ drugs. Red fluorescent pixels also appeared in the fluorescent green edge area. This may have occurred because the porous structure of the GPs caused the ABZ to adhere to the surface openings.

The release of ABZ by the ABZ-GPs under artificial gastric fluid pH and intestinal pH values

The ABZ-GPs releasing ABZ within 10 min showed that the GPs were initially released in a burst; however, their release subsequently decreased after 10 min and ultimately reached an equilibrium state. Notably, the release depends on the solution pH (38,39). The drug release from the GPs was not complete; that is, under an intestinal pH value, the release was rapid and reached 50.0%, while under a gastric fluid pH value, the release was slower and only reached 25.0%. This is due to the loaded drug being protected during the process of passing the human GIT because of the lack of β-1,3-(D) glucanase (34). This indicates that GPs may be able to protect the drugs contained in them from being digested or pumped out. The *in vitro* release of GPs in diverse media follows the Higuchi equation (39) based on data fitting (R^2>0.9800). Based on the data fitting (R^2>0.9900) in the current study, the ABZ release from the ABZ-GPs also conformed to the Higuchi equation.

The dissolution profiles for the formulation obtained under the gastric fluid pH value were compared with the curve obtained under the intestinal tract pH value (*Figure 6*). The results showed that the ABZ-GP nanoparticles had a higher dissolution rate and volume under gastric fluid pH conditions.

ABZ-GPs are engulfed by macrophages

Using the fluorescence-labelled GPs, we were able to investigate the interactions between the macrophages and the ABZ-GPs. According to previously published studies, β-1,3-D-glucan is mainly recognized by dectin-1 and CR3, which are present at high levels in phagocytes (40). This was investigated with *in vitro* phagocytosis assays using

© Annals of Translational Medicine. All rights reserved.

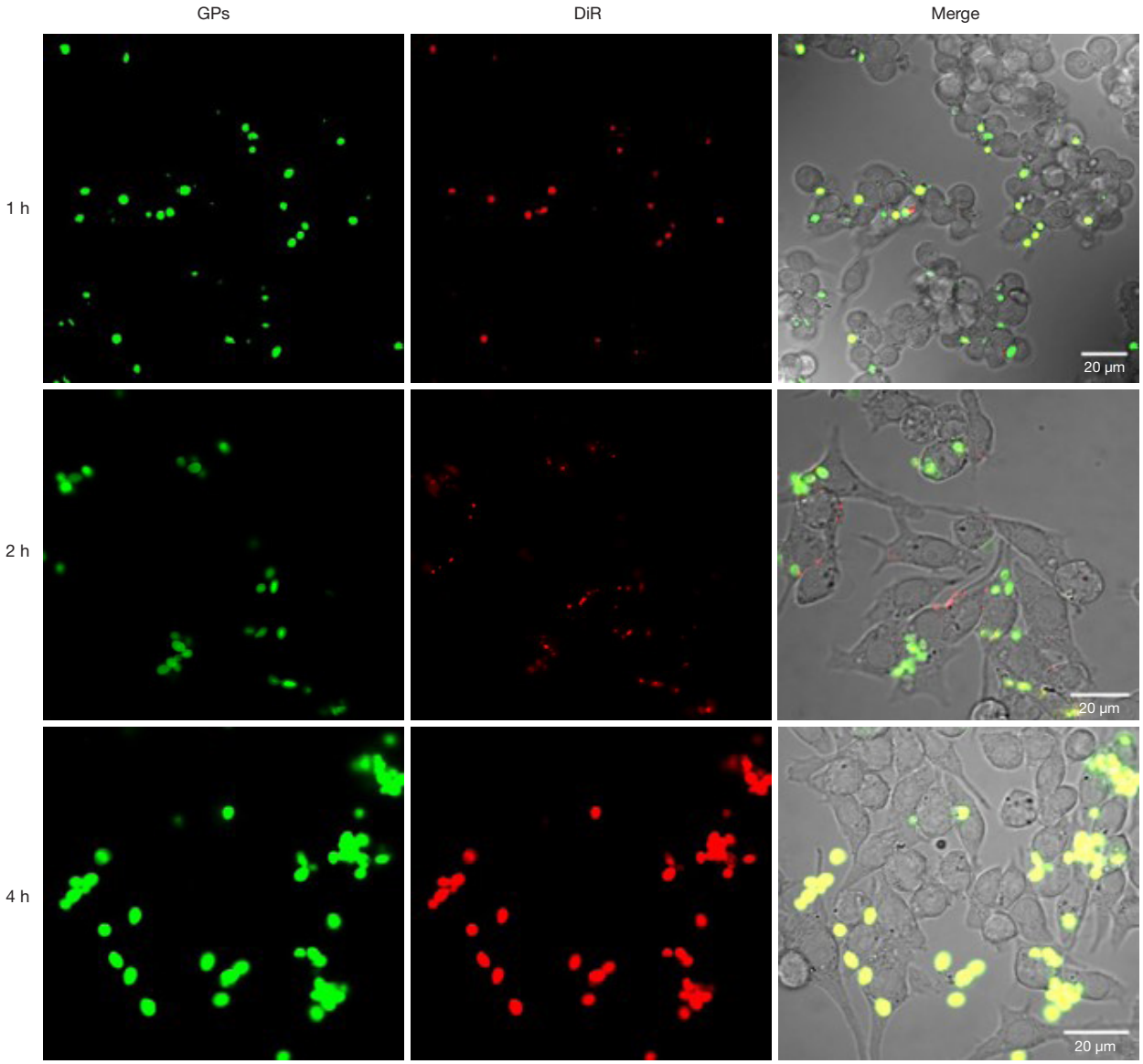

Figure 7 *In vitro* assay of phagocytosis of fluorescence-labelled GPs by RAW 264.7 cells. Confocal imaging of the RAW 264.7 cells treated for 4 h: the first column presents confocal images of the DTAF-labelled GPs at 1, 2, and 4 h, respectively; the second column presents confocal images of the DiR-labelled ABZ-Gd3+-DTPA@BSA at 1, 2 and 4 h; the third column represents images of the double fluorescence-labelled GPs (DiR-labelled peptide core and DTAF-stained GP shell). The confocal images show that the GPs were actively phagocytosed by macrophages. Scale bar =20 μm. GPs, glucan nanoparticles; DTAF, dichlorotriazinyl amino fluorescein; ABZ, albendazole; DTPA, diethylenetriaminepentaacetic acid; BSA, bovine serum albumin.

the mouse macrophage cell line RAW 264.7. When the cells were incubated with ABZ-GPs for 1, 2, and 4 h, the flow ZEISS LSM780 confocal laser microscope analysis indicated that the maximum uptake of the ABZ-GPs occurred at 2 h (*Figure* 7). Thus, ABZ-GPs can be used as a targeting vector for macrophages. From 1 to 2 h, the uptake efficiency of the ABZ-GPs rapidly increased; however, the fluorescence intensity at 4 h was significantly reduced or even lower than that at 1 h. Our findings differ to those of a previous study that reported a maximum uptake of GP capsules by macrophages at 8 h (41). The reason for this difference may be related to the preparation process of the

© Annals of Translational Medicine. All rights reserved.

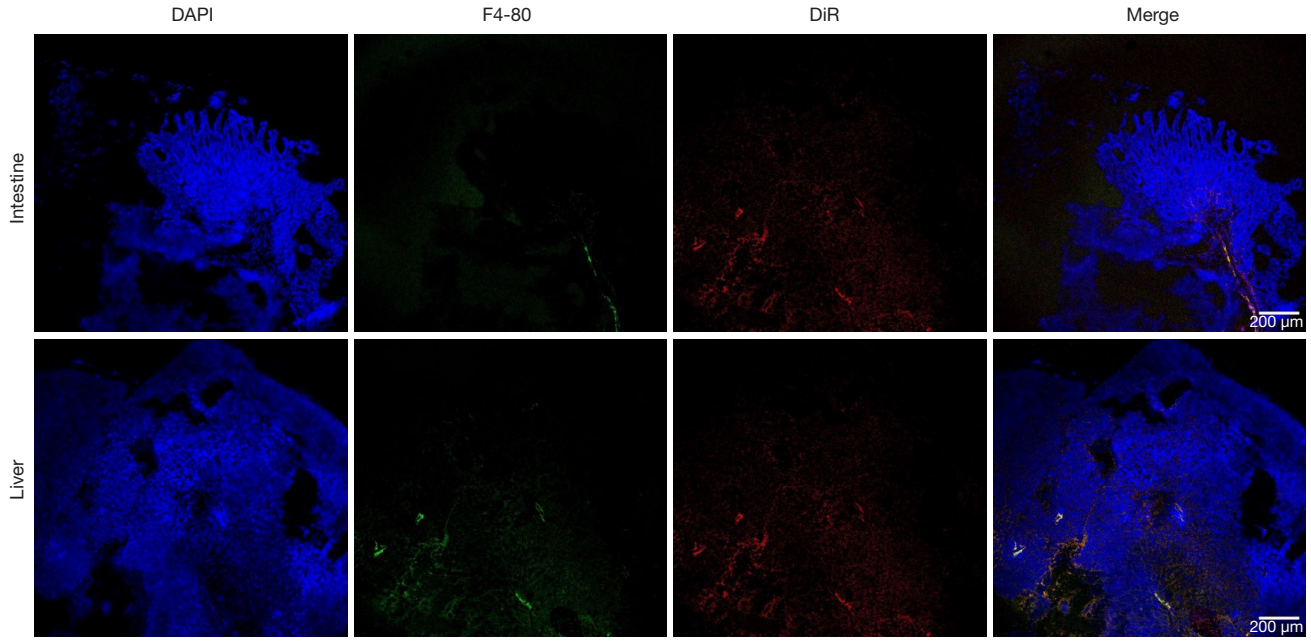

Figure 8 *In vivo* assays of the phagocytosis of fluorescently labelled GPs by small intestine and liver phagocytic cells. The first column shows the small intestine and liver cells labelled with DAPI. The second column shows the F4-80 labelled macrophages in the small intestine and liver tissues. The third column shows the DiR loaded ABZ-Gd^{3+}-DTPA@BSA in the small intestine and liver tissues. The fourth column shows the double fluorescence-labelled phagocytic cells. Scale bar =200 μm. ABZ, albendazole; GPs, glucan nanoparticles; DAPI, 4',6-diamidino-2-phenylindole; DTPA, diethylenetriaminepentaacetic acid; BSA, bovine serum albumin.

Table 1 Pharmacokinetic parameters after intragastric administration in rats

Drug	Standard equation				Linearity range (ng/mL)	
	Plasma	R value	Liver	R value	Plasm	Liver
ABZ	y=0.06x + 0.0893	0.9994	y=0.041x + 0.0153	0.9989	1.56–800.00	1.56–200.00
ABZSO	y=0.0149x – 0.0008	0.9993	y=0.009x – 0.0129	0.9990	1.56–800.00	1.56–200.00

ABZ, albendazole; ABZSO, albendazole sulphoxide.

ABZ-GPs and the characteristics of the drug itself.

We also used healthy Kunming mice to conduct *in vivo* phagocytosis experiments. The ABZ-GP release curves at artificial gastric juice pH and intestinal pH values are shown. Notably, the maximum uptake of ABZ-GPs occurred after 1.5 h (*Figure 6*). The mice were given 50 mg/kg of ABZ-GPs by gavage for 2 h, and the flow Zeiss LSM780 laser confocal microscopy indicated that macrophages in the intestinal mucosa and liver tissues phagocytosed the ABZ-GPs (*Figure 8*). A small number of macrophages were clustered on the surface of selected intestinal mucosa and hepatocytes (i.e., the F4-80 antibody targeted only a few macrophages), indicating low phagocytosis.

Pharmacokinetic profiles and liver targeting

In the pharmacokinetic study, a LC-MS/MS method was established to detect the ABZ-GPs. Based on methodological investigations, this method had a good separation effect, high sensitivity, and high detection efficiency. The specificity of each component of the drug was obvious, and a good linear relationship was detected (*Table 1*). Additionally, the precision, accuracy (*Table 2*), extraction recovery (*Table 3*), and stability (*Table 4*) were all within the allowable error range; thus, this method was successfully applied to investigate the pharmacokinetics of ABZ-GPs in the rat plasma and mouse liver.

© Annals of Translational Medicine. All rights reserved.

Table 2 Recovery and precision

Sample	Concentration (ng/mL)	Precision (%)		Inter-day (RSD, %)		Intra-day (RSD, %)	
		Plasma	Liver	Plasma	Liver	Plasma	Liver
ABZ	12.5	101.47±4.55	100.30±7.38	3.66	4.24	5.39	7.09
	50.0	96.36±4.69	99.96±4.69	8.41	7.57	6.59	5.42
	200.0	103.26±4.44	102.98±2.12	5.68	2.61	4.42	3.00
ABZSO	12.5	100.83±5.84	98.21±3.87	6.39	2.80	5.59	5.07
	50.0	98.48±2.49	102.55±3.34	2.90	3.40	5.51	2.93
	200.0	97.52±6.16	101.70±3.44	2.09	3.19	5.77	3.47

Precision data are presented as mean ± standard deviation; ABZ, albendazole; ABZSO, albendazole sulphoxide; RSD, relative standard deviation.

Table 3 Extraction recovery rate of ABZ and its metabolites in the plasma and liver ($\bar{x} \pm s$, n=5)

Drug	Concentration (ng/mL)	Extraction recovery (%)		RSD (%)	
		Plasma	Liver	Plasma	Liver
ABZ	12.5	97.56±1.80	98.73±6.40	1.84	6.49
	50.0	99.03±2.78	104.75±10.87	3.50	2.81
	200.0	98.98±0.99	101.80±4.98	5.97	1.00
ABZSO	12.5	101.76±3.34	95.73±4.98	4.06	3.28
	50.0	97.66±1.64	95.47±8.24	1.19	1.68
	200.0	101.52±0.78	98.71±3.20	0.94	0.77

Data are presented as mean ± standard deviation. ABZ, albendazole; ABZSO, albendazole sulphoxide; RSD, relative standard deviation.

Table 4 Room temperature stability and freeze-thaw stability of ABZ and its metabolites in the plasma and liver

Drug	Concentration (ng/mL)	RSD (%)											
		Indoors 2 h		Indoors 6 h		Indoors 12 h		Indoors 24 h		Indoors 48 h		Freeze-thaw	
		Plasma	Liver	Plasma	Liver	Plasma	Liver	Plasma	Liver	Plasma	Liver	Plasma	Liver
ABZ	12.5	3.31	3.93	2.54	4.67	4.83	1.85	5.27	6.12	4.81	4.57	4.41	7.08
	50.0	3.94	4.04	4.91	3.52	4.48	4.04	3.06	6.69	3.71	6.26	5.81	4.30
	200.0	3.90	3.94	1.75	2.77	5.63	2.95	3.27	3.89	4.86	1.72	4.40	2.09
ABZSO	12.5	6.98	1.66	3.51	4.02	6.65	4.23	4.78	4.32	7.22	1.90	0.78	4.31
	50.0	1.75	3.31	2.01	5.17	5.83	0.64	5.07	4.98	5.27	1.46	2.84	4.80
	200.0	4.26	4.44	5.94	3.78	6.16	5.13	0.94	3.67	5.43	4.25	4.49	6.49

ABZ, albendazole; ABZSO, albendazole sulphoxide; RSD, relative standard deviation.

The average extraction recovery rate of ABZ and ABZSO in the rat plasma was >95%, and the intra-day and inter-day precision and stability of the relative standard deviations (RSDs) were both <10%. The ABZ absorption (t_{max}) of the ABZ-GP group after the oral administration of the original drug was significantly faster than that of the ABZ group (P<0.01). The elimination of ABZ ($t_{1/2}$) in the ABZ-GP group was also significantly faster than that in the ABZ

© Annals of Translational Medicine. All rights reserved.

Table 5 Main pharmacokinetic parameters of ABZ and ABZSO in the blood (n=10)

Parameter	ABZ		ABZ-GPs	
	ABZ	ABZSO	ABZ	ABZSO
$t_{1/2}$/h	4.69±0.71	2.59±1.73	2.88±1.27#	2.46±0.54
t_{max}/h	2.20±0.35	6.00±1.33	1.70±0.63#	3.90±0.32*
C_{max}/mg·h·L^{-1}	43.15±5.63	783.60±76.54	51.42±9.86	1222.24±81.48*
AUC_0-t/mg·h·L^{-1}	2028.625±152.03	9220.27±939.78	227.03±23.85*	9157.81±869.50
$AUC_{0-\infty}$/mg·h·L^{-1}	2433.40±255.47	10183.36±3225.36	228.42±24.90*	9191.62±904.76
MRT_0-t/h	6.50±0.28	7.60±0.33	4.62±0.45*	5.88±0.41*

Data are presented as mean ± standard deviation. #P<0.05, *P<0.01 versus the ABZ suspension. ABZ, albendazole; ABZ-GPs, albendazole-glucan nanoparticles.

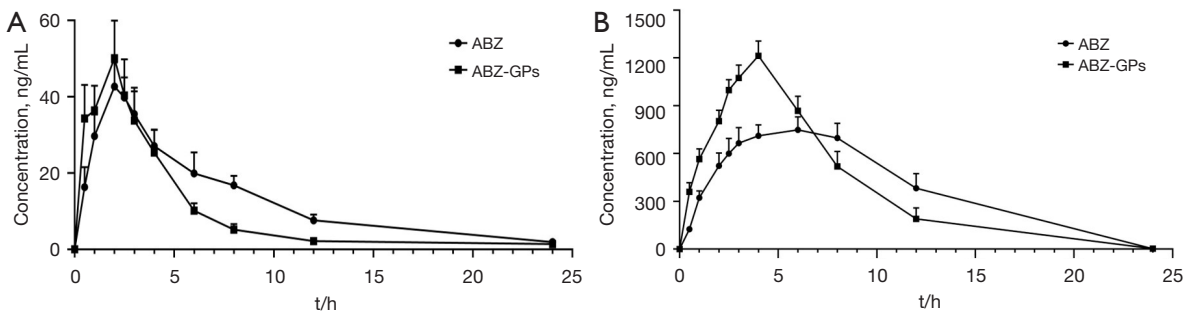

Figure 9 Concentration-time curve in blood of the ABZ-GPs and their metabolites (n=6), (A) ABZ, (B) ABZSO. ABZ-GPs, albendazole-glucan nanoparticles; ABZSO, albendazole sulphoxide.

group (P<0.05), indicating that ABZ-GPs were more readily absorbed and eliminated in the blood than the original ABZ drug. The peak time (t_{max}) of ABZSO of the ABZ-GP group was significantly shorter than that of the ABZ group (P<0.01), however, the retention time of ABZ-GPs in the blood [Mean Retention Time (MRT_0-t)] was significantly shorter in the ABZ-GP group than the ABZ group (P<0.01). A comprehensive analysis of the pharmacokinetic data of the 2 groups revealed that the areas under the curve $(AUCs)_0$-t of ABZ and ABZSO in the ABZ-GP group were significantly smaller than those of the ABZ group. The corresponding pharmacokinetic parameters (*Table 5*) and concentration-time curve (*Figure 9*) demonstrated that the ABZ-GPs were more readily converted to active metabolites than ABZ but were maintained for a shorter time in the blood.

The average extraction recovery rate of ABZ and ABZSO In mouse liver tissue homogenates was approximately 94%, and the intra-day and inter-day precision and stability RSDs were both <10%. After intragastric administration, the livers treated with the original drug (ABZ) and ABZSO had the same peak time (t_{max}); however, the elimination time ($t_{1/2}$) and AUC of the ABZSO in the ABZ-GP group were significantly greater than those in the ABZ group. The AUCs of ABZ and ABZSO in the ABZ-GP group were significantly higher than those in the ABZ group (*Figure 10*). The corresponding pharmacokinetic parameters (*Table 6*) and target parameters (*Table 7*) demonstrated that the ABZ-GPs readily accumulated in the liver tissue and had a good targeting effect.

Distribution of ABZ-GPs in the organs of the mice

On the 5th day, 2D fluorescence images of the mice (*Figure 11A*) were taken on the small animal imager 2 h after the oral gavage. The results showed that the fluorescence was primarily concentrated in the upper left abdomen, and the drug was found to mainly target the liver. We further performed 3D imaging to observe the enrichment of drugs in the liver (*Figure 11B*). The surface topology and signal

© Annals of Translational Medicine. All rights reserved.

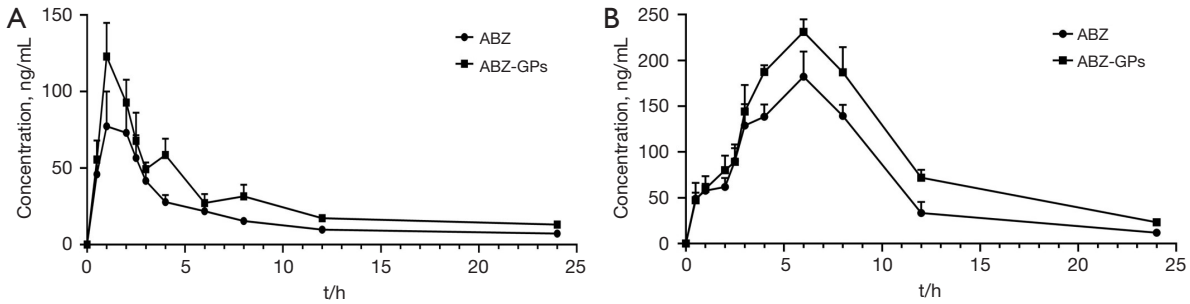

Figure 10 Concentration-time curve in the liver of the ABZ-GPs and their metabolites (n=6), (A) ABZ, (B) ABZSO. ABZ-GPs, albendazole-glucan nanoparticles; ABZSO, albendazole sulphoxide.

Table 6 Main pharmacokinetic parameters of ABZ and ABZSO in the liver (n=5)

Parameter	ABZ		ABZ-GPs	
	ABZ	ABZSO	ABZ	ABZSO
$t_{1/2}$/h	5.30	4.51	4.53	5.38
t_{max}/h	1.00	6.00	1.00	6.00
C_{max}/mg·h·L^{-1}	77.31	182.18	122.84	231.02
AUC_0-t/mg·h·L^{-1}	448.54	1,581.98	712.682	2,299.54
$AUC_{0-\infty}$/mg·h·L^{-1}	464.17	1,657.91	730.56	2,480.15
MRT_0-t/h	6.96	7.45	7.58	8.37

ABZ, albendazole; ABZ-GPs, albendazole-glucan nanoparticles; ABZSO, albendazole sulphoxide.

Table 7 The target parameters (Ce and TI) of the 2 preparations in the liver (n=5)

Drug	Ce	TI
ABZ	1.59	1.57
ABZSO	1.27	1.50

ABZ, albendazole; ABZ-GPs, albendazole-glucan nanoparticles; Ce, peak concentration ratio; TI, targeting index; Ce = (C_{max}) ABZ/(C_{max}) ABZ-GPs, TI = ($AUC_{0-\infty}$) ABZ/($AUC_{0-\infty}$) ABZ-GPs. ABZSO, albendazole sulphoxide

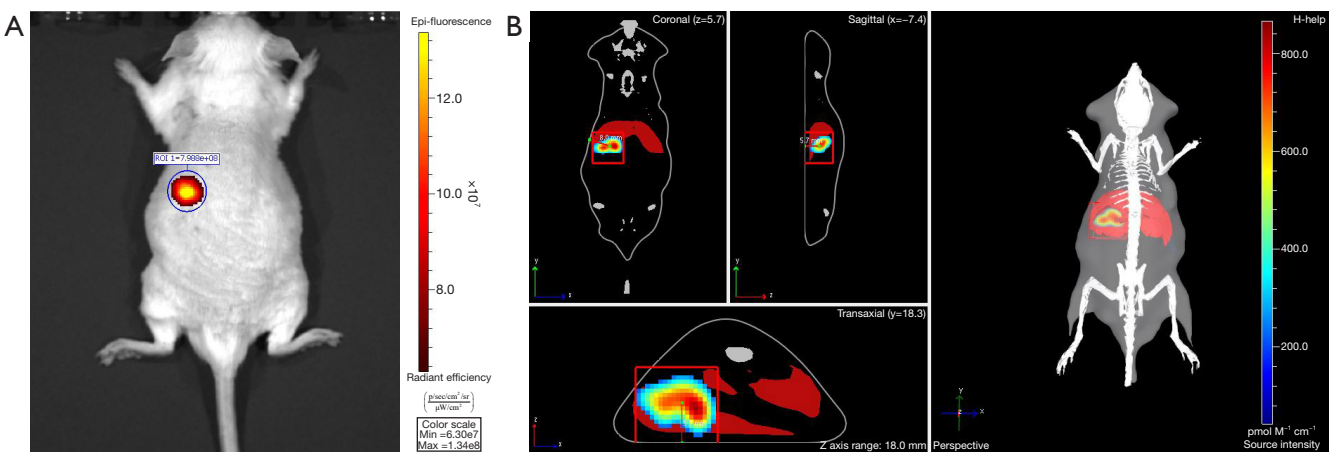

Figure 11 The small animal live imaging instrument detected the organ targeting of ABZ-GPs. (A) 2D near-infrared fluorescence imaging, (B) 3D near-infrared fluorescence imaging. ABZ-GPs, albendazole-glucan nanoparticles.

© Annals of Translational Medicine. All rights reserved.

source were reconstructed by scanning the 2D image of each mouse in the white-light mode to detect and analyze the coronal and sagittal planes of the mouse body, the cross-section of the mouse abdomen, and the drug distribution in the mouse abdomen. Based on the 3D imaging results, after the drug had been orally ingested, it gradually accumulated in the liver via diffusion; however, a small amount was destroyed. This result indicated a specific targeting effect on the liver and supports the conclusion of drug liver targeting.

Discussion

To the best of our knowledge, our study was the first to prepare ABZ-GPs using FDA-approved GPs as carriers and modified BSA with DTPA and gadolinium nitrate [$Gd(NO_3)_3{\cdot}6H_2O$]. We found that the ABZ-GPs did not aggregate, displayed spherical characteristics, had a considerable drug content, and had a high packaging efficiency. Moreover, the ABZ-GPs were recognized by specific receptors on the surface of macrophages and act as a targeting carrier for macrophages, thereby improving the targeting of the drug to the liver.

With the development of nanotechnology, the use of passive targeting to achieve targeted drug delivery has been extensively studied. The FDA has approved the targeted delivery of drugs with GPs, and this is the fastest way to realize the industrialization and clinical application of the targeted delivery of drugs. Thus it's worth exploring. The hollow structure of GPs serves as a carrier, while the porous structure of the surface not only protects the internal molecules to a certain extent, but also ensures the slow release of the drug. Additionally, the hollow and porous structure of the GPs enables the transport of single-component or multi-component drugs in large doses. This advantage is unmatched by other drug carriers reported to date (42,43). However, cell wall-derived GPs has low content and complex production process that prevents mass production of GPs. Therefore, we need to increase the content of GPs by means of physical or chemical induction or gene knockout. In addition, ABZ-GPs as a clinical drug due to the strong immunomodulatory effect of GPs, ABZ-GPs should be used with caution in patients with echinococcosis who are taking immunosuppressive agents, diabetes or related hypoglycemic drugs.

In our experiments, the macrophages internalized the ABZ-GPs, which may be specifically recognized by GP receptors that are highly expressed on the surface of macrophages, such as dectin-1 or CR_3 (CD_{11b}/CD_{18}). The ABZ-GPs are phagocytosed intracellularly, and their biodegradation only occurs through oxidative lysis in polymorphonuclear leukocytes and monocytes/macrophages after being absorbed by the intestine (44,45) where the loaded drug can be released. Thus, the ABZ-GPs can be used as targeting vectors for macrophages (46,47). Studies have shown that GPs can preferentially protect encapsulated polypeptides from degradation in gastric acid and intestinal juice, while allowing them to be phagocytosed by macrophages in the intestines and delivered systemically. Once inflammation occurs, they will be recruited to the inflammation site via chemokine and cytokine action (48-50). This is consistent with the results of the present experiment that showed that ABZ-GPs protect ABZ from digestion or pumping by gastric juice pH and intestinal pH, and can be recognized by macrophages, and then combined and internalized into the macrophages. The above characteristics of GPs compared with the natural non-toxic chitosan, which is also used as a drug carrier, Chitosan improves the permeability of epithelial cell biofilms to drugs through its adhesion and degradation, prolonged contact of drugs and intestinal absorption parts, reducing the drug from the intestinal excretion in the form of technical, to improve the concentration of drug in plasma and liver. Thus, the indigestibility and relative stability of GPs in the intestinal tract and their immunomodulatory effects make them ideal carriers for various compounds.

Additionally, the LC-MS/MS method revealed that the peak time (t_{max}) for the elimination half-life time ($t_{1/2}$) of the ABZ-GPs in the rat plasma was significantly shorter than that of the ABZ group. There were no significant changes in the C_{max} between the 2groups; however, the difference between the ABZ and ABZSO values of the AUC_0-t and MRT were significantly lower than those of the ABZ group, indicating that the ABZ-GPs were absorbed and reached the C_{max} quickly in rats. However, the mean retention time in the blood was shorter, which may be related to the dissolution of ABZ carried by GPs *in vivo*. The ABZ-GPs in this study only altered the absorption rate *in vivo*, but were unable to alter or increase the plasma concentration and $AUC_{0-\infty}$, which may be related to the characteristics of the GPs and their dissolution *in vivo*.

Studies have shown that the GPs can effectively prevent enzymatic digestion and the immune clearance of the drug carrier when the drug reaches the target tissue/cell (51). Thus, the GPs enhance the stability of the drug delivery system and reduce the accumulation of drugs in the blood circulation (52). The encapsulation of poorly soluble drugs

© Annals of Translational Medicine. All rights reserved.

in yeast GPs also improves dispersion and dissolution properties (53). The results of the mouse liver targeting experiments showed that the t_{max} (1.00 h, 6.00 h) of ABZ and the active ingredient ABZSO in the ABZ-GP group and ABZ group were the same. Moreover, there was no significant difference in the C_{max} between the 2 groups, indicating that ABZ-GPs were metabolized in the liver (i.e., ABZ and the metabolic properties of ABZSO did not change significantly). However, the Mean Retention Time (MRT_0-t), elimination half-life ($t_{1/2}$), and $AUC_{0-\infty}$ of the ABZ-GPs in the liver of the mice were significantly greater than those of the mice in the ABZ group. Combined with the 2D and 3D fluorescence real-time imaging after treatment with ABZ-GPs, our results indicate that the circulation time, bioavailability, and curative effect of ABZ-GPs in the liver were significantly improved.

Based on our results, as a carrier, the GPs can achieve safe and efficient targeted drug delivery by simple oral administration, and have universal applicability to other types of drugs. Following the discovery of other anti-hydatid drugs, this method could be used to carry drugs with different effects at a fixed ratio and would be safer for targeting and delivery to the lesion site. Unfortunately, we did not instrumentally detect whether ABZ-GPs enter vesicles (i.e., we did not gather data on whether ABZ-GPs can enter hydatid vesicles) and thus we were unable to determine the killing effect of ABZ-GPs on echinococcosis. Thus, future iterations of ABZ-GPs may exhibit an even greater potency. Due to the synergistic effect between ABZ and the GPs and the enhancement of the anti-hydatid and immune stimulation effects, the control of the disease can be realized, and new scientific explorations can be made to improve the quality of life of patients with hydatid diseases.

Conclusions

ABZ-GPs, as drug carriers, are biodegradable, have good tissue compatibility, and low toxicity (or non-toxicity), and can be used in a macrophage-targeted carrier drug delivery system. In our mouse liver targeting experiment, fluorescence imaging and the accumulation of drugs in the liver indicated that GPs can be used as carriers to achieve the targeted transport of ABZ, which in turn can be used for the targeted therapy of liver echinococcosis.

Acknowledgments

The authors would like to thank the Basic Medical Research Center, School of Medicine, Qinghai University for providing the experimental site. We are also grateful to Dr. Xu Zhang (Tsinghua University, People's Republic of China) for his drug research and preparation, and Dr. Qiangqiang Jia (Qinghai University, People's Republic of China) for his technical assistance in the use of the Fourier transform ultra-high-resolution LC/MS instrument.

Funding: This work was supported by the National Natural Science Foundation of China (grant No. 81960451), Qinghai Provincial Department of Science and Technology (grant No. 2019-ZJ-7055) and Qinghai University Medical College Team Project Foundation (grant No. 2018-kyt-2). The sponsor did not have any role in the study design, the collection, analysis, or interpretation of the data, the writing of the manuscript, or the decision to submit the article for publication.

Footnote

Reporting Checklist: The authors have completed the ARRIVE reporting checklist. Available at https://atm.amegroups.com/article/view/10.21037/atm-22-5299/rc

Data Sharing Statement: Available at https://atm.amegroups.com/article/view/10.21037/atm-22-5299/dss

Conflicts of Interest: All authors have completed the ICMJE uniform disclosure form (available at https://atm.amegroups.com/article/view/10.21037/atm-22-5299/coif). The authors have no conflicts of interest to declare.

Ethical Statement: The authors are accountable for all aspects of the work in ensuring that questions related to the accuracy or integrity of any part of the work are appropriately investigated and resolved. Animal experiments were approved by the Research Ethics Committee of the Affiliated Hospital of Qinghai University (approval No. AF-RHEC-0062-01) and in compliance with institutional guidelines for the care and use of animals.

Open Access Statement: This is an Open Access article distributed in accordance with the Creative Commons Attribution-NonCommercial-NoDerivs 4.0 International License (CC BY-NC-ND 4.0), which permits the non-commercial replication and distribution of the article with the strict proviso that no changes or edits are made and the original work is properly cited (including links to both the formal publication through the relevant

© Annals of Translational Medicine. All rights reserved.

DOI and the license). See: https://creativecommons.org/licenses/by-nc-nd/4.0/.

References

1. Ben Khelil M, Allouche M, Banasr A, et al. Sudden death due to hydatid disease: a six-year study in the northern part of Tunisia. J Forensic Sci 2013;58:1163-70.
2. Zhang MY, Wu WP. Advances in study of the burden of echinococcosis in China and elsewhere around the world. J Pathog Biol 2017;12:473-5.
3. Jura H, Bader A, Hartmann M, et al. Hepatic tissue culture model for study of host-parasite interactions in alveolar echinococcosis. Infect Immun 1996;64:3484-90.
4. Craig PS, Giraudoux P, Wang ZH, et al. Echinococcosis transmission on the Tibetan Plateau. Adv Parasitol 2019;104:165-246.
5. Siles-Lucas M, Casulli A, Cirilli R, et al. Progress in the pharmacological treatment of human cystic and alveolar echinococcosis: Compounds and therapeutic targets. PLoS Negl Trop Dis 2018;12:e0006422.
6. Kourentas A, Vertzoni M, Khadra I, et al. Evaluation of the Impact of Excipients and an Albendazole Salt on Albendazole Concentrations in Upper Small Intestine Using an In Vitro Biorelevant Gastrointestinal Transfer (BioGIT) System. J Pharm Sci 2016;105:2896-903.
7. Zhao J, Gao HJ, Wang JH. Chinese invention patent about anti-parasitic drug albendazole. Zhongguo Ji Sheng Chong Xue Yu Ji Sheng Chong Bing Za Zhi 2012;30:152-156+159.
8. Liu Y, Wang XQ, Ren WX, et al. Novel albendazole-chitosan nanoparticles for intestinal absorption enhancement and hepatic targeting improvement in rats. J Biomed Mater Res B Appl Biomater 2013;101:998-1005.
9. Pensel PE, Castro S, Allemandi D, et al. Enhanced chemoprophylactic and clinical efficacy of albendazole formulated as solid dispersions in experimental cystic echinococcosis. Vet Parasitol 2014;203:80-6.
10. Chai J, Menghebat, Wei J, et al. Observations on clinical efficacy of albendazole emulsion in 264 cases of hepatic cystic echinococcosis. Parasitol Int 2004;53:3-10.
11. Mirza Z, Soto ER, Dikengil F, et al. Beta-Glucan Particles as Vaccine Adjuvant Carriers. Methods Mol Biol 2017;1625:143-57.
12. Treml J, Šalamúnová P, Hanuš J, et al. The effect of curcumin encapsulation into yeast glucan particles on antioxidant enzyme expression in vitro. Food Funct 2021;12:1954-7.
13. Šalamúnová P, Cupalová L, Majerská M, et al. Incorporating natural anti-inflammatory compounds into yeast glucan particles increases their bioactivity in vitro. Int J Biol Macromol 2021;169:443-51.
14. Ma M, Li Y, Chen J, et al. High-cell-density cultivation of the flagellate alga Poterioochromonas malhamensis for biomanufacturing the water-soluble β-1,3-glucan with multiple biological activities. Bioresour Technol 2021;337:125447.
15. Šalamúnová P, Saloň I, Ruphuy G, et al. Evaluation of β-glucan particles as dual-function carriers for poorly soluble drugs. Eur J Pharm Biopharm 2021;168:15-25.
16. Brown GD, Gordon S. Immune recognition. A new receptor for beta-glucans. Nature 2001;413:36-7.
17. Beller DI, Springer TA, Schreiber RD. Anti-Mac-1 selectively inhibits the mouse and human type three complement receptor. J Exp Med 1982;156:1000-9.
18. Means TK, Mylonakis E, Tampakakis E, et al. Evolutionarily conserved recognition and innate immunity to fungal pathogens by the scavenger receptors SCARF1 and CD36. J Exp Med 2009;206:637-53.
19. Iossifova Y, Reponen T, Sucharew H, et al. Use of (1-3)-beta-d-glucan concentrations in dust as a surrogate method for estimating specific fungal exposures. Indoor Air 2008;18:225-32.
20. Plavcová Z, Šalamúnová P, Saloň I, et al. Curcumin encapsulation in yeast glucan particles promotes its anti-inflammatory potential in vitro. Int J Pharm 2019;568:118532.
21. Xie Y, Jiang S, Xia F, et al. Glucan microparticles thickened with thermosensitive gels as potential carriers for oral delivery of insulin. J Mater Chem B 2016;4:4040-8.
22. Xie Y, Hu X, He H, et al. Tracking translocation of glucan microparticles targeting M cells: implications for oral drug delivery. J Mater Chem B 2016;4:2864-73.
23. Aouadi M, Tesz GJ, Nicoloro SM, et al. Orally delivered siRNA targeting macrophage Map4k4 suppresses systemic inflammation. Nature 2009;458:1180-4.
24. Soto ER, Ostroff GR. Characterization of multilayered nanoparticles encapsulated in yeast cell wall particles for DNA delivery. Bioconjug Chem 2008;19:840-8.
25. Tesz GJ, Aouadi M, Prot M, et al. Glucan particles for selective delivery of siRNA to phagocytic cells in mice. Biochem J 2011;436:351-62.
26. Soto ER, O'Connell O, Dikengil F, et al. Targeted Delivery of Glucan Particle Encapsulated Gallium Nanoparticles

© Annals of Translational Medicine. All rights reserved.

Inhibits HIV Growth in Human Macrophages. J Drug Deliv 2016;2016:8520629.
27. Sun Y, Duan B, Chen H, et al. A Novel Strategy for Treating Inflammatory Bowel Disease by Targeting Delivery of Methotrexate through Glucan Particles. Adv Healthc Mater 2020;9:e1901805.
28. Rotrekl D, Šalamúnová P, Paráková L, et al. Composites of yeast glucan particles and curcumin lead to improvement of dextran sulfate sodium-induced acute bowel inflammation in rats. Carbohydr Polym 2021;252:117142.
29. Soares E, Groothuismink ZMA, Boonstra A, et al. Glucan Particles Are a Powerful Adjuvant for the HBsAg, Favoring Antiviral Immunity. Mol Pharm 2019;16:1971-81.
30. Whelan AO, Flick-Smith HC, Homan J, et al. Protection induced by a Francisella tularensis subunit vaccine delivered by glucan particles. PLoS One 2018;13:e0200213.
31. Vetvicka V, Vannucci L, Sima P. β-glucan as a new tool in vaccine development. Scand J Immunol 2020;91:e12833.
32. Colaço M, Panão Costa J, Borges O. Glucan Particles: Choosing the Appropriate Size to Use as a Vaccine Adjuvant. Methods Mol Biol 2022;2412:269-80.
33. Wang DX. The Role and Mechanism of Macrophage Polarization in Hepatic Alveolar Echinococcosis. Qinghai University. 2018. Available online: https://kns.cnki.net/KCMS/ detail/detail.aspx?dbname=CMFD201802&filename=1018995433.nh
34. De Smet R, Demoor T, Verschuere S, et al. β-Glucan microparticles are good candidates for mucosal antigen delivery in oral vaccination. J Control Release 2013;172:671-8.
35. Pandya JJ, Sanyal M, Shrivastav PS. Simultaneous densitometric determination of anthelmintic drug albendazole and its metabolite albendazole sulfoxide by HPTLC in human plasma and pharmaceutical formulations. Biomed Chromatogr 2017. doi: 10.1002/bmc.3947.
36. Chhonker YS, Edi C, Murry DJ. LC-MS/MS method for simultaneous determination of diethylcarbamazine, albendazole and albendazole metabolites in human plasma: Application to a clinical pharmacokinetic study. J Pharm Biomed Anal 2018;151:84-90.
37. Loura LM, Fedorov A, Prieto M. Partition of membrane probes in a gel/fluid two-component lipid system: a fluorescence resonance energy transfer study. Biochim Biophys Acta 2000;1467:101-12.
38. Kulkarni RV, Mutalik S, Mangond BS, et al. Novel interpenetrated polymer network microbeads of natural polysaccharides for modified release of water soluble drug: in vitro and in vivo evaluation. J Pharm Pharmacol 2012;64:530-40.
39. Reza MS, Quadir MA, Haider SS. Comparative evaluation of plastic, hydrophobic and hydrophilic polymers as matrices for controlled-release drug delivery. J Pharm Pharm Sci 2003;6:282-91.
40. Goodridge HS, Reyes CN, Becker CA, et al. Activation of the innate immune receptor Dectin-1 upon formation of a 'phagocytic synapse'. Nature 2011;472:471-5.
41. Zhang X, Zhao Y, Xu Y, et al. In situ self-assembly of peptides in glucan particles for macrophage-targeted oral delivery. J Mater Chem B 2014;2:5882-90.
42. Figueiredo S, Moreira JN, Geraldes CF, et al. Yeast cell wall particles: a promising class of nature-inspired microcarriers for multimodal imaging. Chem Commun (Camb) 2011;47:10635-7.
43. Garello F, Stefania R, Aime S, et al. Successful entrapping of liposomes in glucan particles: an innovative micron-sized carrier to deliver water-soluble molecules. Mol Pharm 2014;11:3760-5.
44. Bajgar A, Saloň I, Krejčová G, et al. Yeast glucan particles enable intracellular protein delivery in Drosophila without compromising the immune system. Biomater Sci 2019;7:4708-19.
45. Nono I, Ohno N, Masuda A, et al. Oxidative degradation of an antitumor (1-3)-beta-D-glucan, grifolan. J Pharmacobiodyn 1991;14:9-19.
46. Rotrekl D, Devriendt B, Cox E, et al. Glucan particles as suitable carriers for the natural anti-inflammatory compounds curcumin and diplacone - Evaluation in an ex vivo model. Int J Pharm 2020;582:119318.
47. Willment JA, Marshall AS, Reid DM, et al. The human beta-glucan receptor is widely expressed and functionally equivalent to murine Dectin-1 on primary cells. Eur J Immunol 2005;35:1539-47.
48. Möhwald M, Pinnapireddy SR, Wonnenberg B, et al. Aspherical, Nanostructured Microparticles for Targeted Gene Delivery to Alveolar Macrophages. Adv Healthc Mater 2017. doi: 10.1002/adhm.201700478.
49. Na YR, Stakenborg M, Seok SH, et al. Macrophages in intestinal inflammation and resolution: a potential therapeutic target in IBD. Nat Rev Gastroenterol Hepatol 2019;16:531-43.
50. Rios de la Rosa JM, Tirella A, Gennari A, et al. The CD44-Mediated Uptake of Hyaluronic Acid-Based Carriers in Macrophages. Adv Healthc Mater 2017.
51. Chirizzi C, Dastrù W, Castelli DD, et al. Glucan

© Annals of Translational Medicine. All rights reserved.

particles loaded with fluorinated emulsions: A Sensitivity Improvement for the Visualization of phagocytic Cells by 19F-MRI. Curr Mol Imaging 2015;4:29-34.
52. Varshosaz J. Dextran conjugates in drug delivery. Expert Opin Drug Deliv 2012;9:509-23.
53. Ruphuy G, Saloň I, Tomas J, et al. Encapsulation of poorly soluble drugs in yeast glucan particles by spray drying improves dispersion and dissolution properties. Int J Pharm 2020;576:118990.

(English Language Editor: L. Huleatt)

Cite this article as: Liu Y, Yang H, Zhu J, Yang Z, Zhao L, Zhang X, Zhang H. Novel albendazole-glucan particles for enhancing intestinal absorption and improving hepatic targeting. Ann Transl Med 2022;10(24):1312. doi: 10.21037/atm-22-5299

© Annals of Translational Medicine. All rights reserved.